

27 66

**From: FUNDAMENTAL PROCESSES OF ATOMIC DYNAMICS**  
Edited by J. S. Briggs, H. Kleinpoppen, and H. O. Lutz  
(Plenum Publishing Corporation, 1988)

SHAPE RESONANCES IN MOLECULAR FIELDS\*

J. L. Dehmer,<sup>†</sup> D. Dill,<sup>#</sup> and A. C. Parr,<sup>§</sup>

<sup>†</sup>Argonne National Laboratory, Argonne, IL 60439

<sup>#</sup>Department of Chemistry, Boston University, Boston, MA 02215

<sup>§</sup>National Bureau of Standards, Gaithersburg, MD 20899

I. INTRODUCTION

The last two decades have witnessed remarkable progress in characterizing dynamical aspects of molecular photoionization<sup>1,2</sup> and electron-molecule scattering<sup>2,3</sup> processes. The general challenge is to gain physical insight into the processes occurring during the excitation, evolution, and decay of the excited molecular complex. Of particular interest in this context are the uniquely molecular aspects resulting from the anisotropy of the molecular field and from the interplay among rovibronic modes. Throughout this work, special attention is invariably drawn to resonant processes, in which the excited system is temporarily trapped in a quasibound resonant state. Such processes tend to amplify the more subtle dynamics of excited molecular states and are often displayed prominently against non-resonant behavior in various physical observables.

One very vigorous stream of work has involved shape resonances in molecular systems. These resonances are quasibound states in which a particle is temporarily trapped by a potential barrier, through which it may eventually tunnel and escape. In molecular fields, such states can result from so-called "centrifugal barriers," which block the motion of otherwise free electrons in certain directions, trapping them in a region of space with molecular dimensions. Over the years, this basic resonance mechanism has been found to play a prominent role in a variety of processes in molecular physics, thus becoming a major theme in the study of molecular photoionization and electron-molecule scattering processes. As discussed more fully in later sections, the expanding interest in shape resonant phenomena has arisen from a few key factors:

First, shape resonance effects are being identified in the spectra of a growing and diverse collection of molecules and now appear to be active somewhere in the observable properties of most small (nonhydride) molecules. Examples of the processes which exhibit shape resonant

\*Work supported in part by the U.S. Department of Energy, Office of Health and Environmental Research, under Contract W-31-109-Eng-38. Accordingly the U.S. Government retains a nonexclusive, royalty-free license to publish or reproduce the published form of this contribution, or allow others to do so, for U.S. Government purposes.

effects are x-ray and VUV absorption spectra, photoelectron branching ratios and photoelectron angular distributions (including vibrationally resolved), Auger electron angular distributions, elastic electron scattering, vibrational excitation by electron impact, and so on. Thus concepts and techniques developed in this connection can be used extensively in molecular physics.

Second, being quasibound inside a potential barrier on the perimeter of the molecule, such resonances are localized, have enhanced electron density in the molecular core, and are uncoupled from the external environment of the molecule. This localization often produces intense, easily studied spectral features, while suppressing non-resonant and/or Rydberg structure, and as discussed more fully below, has a marked influence on vibrational motion. In addition, localization causes much of the conceptual framework developed for shape resonances in free molecules to apply equally well to photoionization and electron scattering and to other states of matter such as adsorbed molecules, molecular crystals, and ionic solids.

Third, resonant trapping by a centrifugal barrier often imparts a well-defined orbital momentum character to the escaping electron. This can be directly observed, e.g. by angular distributions of scattered electrons or photoelectron angular distributions from oriented molecules, and shows that the centrifugal trapping mechanism has physical meaning and is not merely a theoretical construct. Recent case studies have revealed trapping of  $l = 1$  to  $l = 5$  components of continuum molecular wave functions. The purely molecular origin of the great majority of these cases is illustrated by the prototype system  $N_2$  discussed in Section III.

Fourth, the predominantly one-electron nature of the phenomena lends itself to theoretical treatment by realistic, independent electron methods,<sup>2,4-11</sup> with the concomitant flexibility in terms of complexity of molecular systems, energy ranges, and alternative physical processes. This has been a major factor in the rapid exploration in this area. Continuing development of computational schemes also holds the promise of elevating the level of theoretical work on molecular photoionization and electron-molecule scattering and, in so doing, to test and quantify many of the independent-electron results and to proceed to other circumstances such as coupled channels, multiply excited states, etc. where the simpler schemes become invalid.

In the remainder of this article, we review the study of shape resonances in molecular fields with a fairly broad perspective, beginning with a discussion of the rudimentary concepts and ending with a comment on current challenges: Section II begins by presenting an example of dramatic shape resonance behavior, involving x-ray spectra of  $SF_6$ . Section III discusses the basic shape resonance mechanism in simple terms. Section IV treats shape-resonance-induced vibrational effects. Section V discusses connections between shape resonances in various settings, principally the connection between shape resonances in electron-molecule scattering and molecular photoionization. Finally, Section VI outlines the progress and prospects in this stream of work from a broader point-of-view, including some less transparent cases which represent current challenges to our understanding.

## II. A DRAMATIC EXAMPLE OF SHAPE RESONANT BEHAVIOR

Among the earliest and still possibly the most dramatic examples of shape resonance effects in molecules are the photoabsorption spectra of

the sulfur K-<sup>12,13</sup> and L-shells<sup>13-16</sup> in SF<sub>6</sub>. The sulfur L-shell absorption spectra of SF<sub>6</sub> and H<sub>2</sub>S are shown in Fig. 1 to illustrate the type of phenomena that originally drew attention to this area. In Fig. 1 both spectra are plotted on a photon energy scale referenced to the sulfur L-shell ionization potential (IP) which is chemically shifted by a few eV in the two molecular environments, but lies near  $h\nu \sim 175$  eV. The ordinates represent relative photoabsorption cross sections and have been adjusted so that the integrated oscillator strength for the two systems is roughly equal in this spectral range, since absolute normalizations are not known. The H<sub>2</sub>S spectrum is used here as a "normal" reference spectrum since hydrogen atoms normally do not contribute appreciably to shape resonance effects and, in this particular context, can be regarded as weak perturbations on the inner-shell spectra of the heavy atom. Indeed, the photoabsorption spectrum exhibits what appears to be a

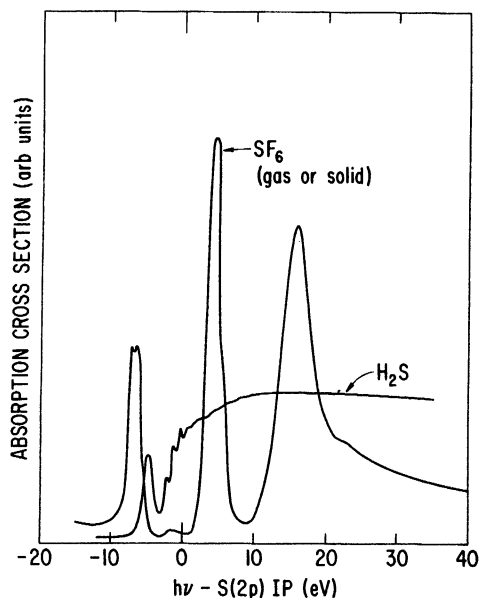


Fig. 1. Photoabsorption spectra of H<sub>2</sub>S (taken from Ref. 15) and SF<sub>6</sub> (taken from Ref. 16) near the sulfur L<sub>2,3</sub> edge.

valence transition, followed by partially resolved Rydberg structure, which converges to a smooth continuum. The gradual rise at threshold is attributable to the delayed onset of the "2p → εd" continuum which, for second row atoms, will exhibit a delayed onset prior to the occupation of the 3d subshell. This is the qualitative behavior one might well expect for the absorption spectrum of a core level.

In sharp contrast to this, the photoabsorption spectrum of the same sulfur 2p subshell in SF<sub>6</sub> shows no vestige of the "normal" behavior just described. Instead three intense, broad peaks appear, one below the ionization threshold and two above, and the continuum absorption cross section is greatly reduced elsewhere. Moreover, no Rydberg structure is

apparent, although an infinite number of Rydberg states must necessarily be associated with any molecular ion. Actually, Rydberg states were detected<sup>17</sup> superimposed on the weak bump below the IP using photographic detection, but obviously these states are extremely weak in this spectrum. This radical reorganization of the oscillator strength distribution was interpreted<sup>18</sup> as potential barrier effects in SF<sub>6</sub>, resulting in three shape-resonantly enhanced final state features of a<sub>1g</sub>, t<sub>2g</sub>, and e<sub>g</sub> symmetry, in order of increasing energy. Another shape resonant feature of t<sub>1u</sub> symmetry is prominent in the sulfur K-shell spectrum<sup>12</sup> and, in fact, is believed to be responsible for the weak feature just below the IP in Fig. 1. Hence, four prominent features occur in the photoexcitation spectrum of SF<sub>6</sub> as a consequence of potential barriers caused by the molecular environment of the sulfur atom. Another significant observation<sup>16</sup> is that the SF<sub>6</sub> curve in Fig. 1 represents both gaseous and solid SF<sub>6</sub>, within experimental error bars. This is definitive evidence that the resonances are eigenfunctions of the potential well inside the barrier, and are effectively uncoupled from the molecule's external environment.

This beautiful empirical evidence had a strong stimulating effect in the study of shape resonances in molecular photoionization, just as early observations of the  $\pi_g$  shape resonance in elastic e-N<sub>2</sub> scattering did in the electron-molecule scattering field.<sup>3,19</sup>

### III. BASIC PROPERTIES

The central concept in shape resonance phenomena is the single-channel, barrier-penetration model familiar from introductory quantum mechanics. In fact, the name "shape resonance" means simply that the resonance behavior arises from the "shape," i.e. the barrier and associated inner and outer wells, of a local potential. The basic shape resonance mechanism is illustrated schematically<sup>20</sup> in Fig. 2. There, an effective potential for an excited and/or unbound electron is shown to have an inner well at small distances, a potential barrier at intermediate distances, and an outer well (asymptotic form not shown) at large separations. In the context of molecular photoionization, this would be a one-dimensional abstraction of the effective potential for the photoelectron in the field of a molecular ion. Accordingly, the inner well would be formed by the partially screened nuclei in the molecular core and would therefore be highly anisotropic and would overlap much of the molecular charge distribution, i.e., the initial states of the photoionization process. The barrier, in all well-documented cases, is a so-called centrifugal barrier (other forces such as repulsive exchange forces, high concentrations of negative charge, etc., may also contribute, but have not yet been documented to be pivotal in the molecular systems studied to date). This centrifugal barrier derives from a competition between repulsive centrifugal forces and attractive electrostatic forces and usually (but not always) resides on the perimeter of molecular charge distributions where the centrifugal forces can compete effectively with electrostatic forces. Similar barriers are known for d- and f-waves in atomic fields,<sup>21</sup> however the  $\ell$  (orbital angular momentum) character of resonances in molecular fields tends to be higher than those of constituent atoms owing to the larger spatial extent of molecular charge distributions, e.g., see discussion in connection with N<sub>2</sub> photoionization below. The outer well lies outside the molecule where the Coulomb potential ( $\sim -r^{-1}$ ) of the molecular ion again dominates the centrifugal terms ( $\sim r^{-2}$ ) in the potential. We stress that this description has been radically simplified to convey the essential aspects of the underlying physics. In reality effective barriers to electron motion in molecular fields occur for particular  $\ell$  components of

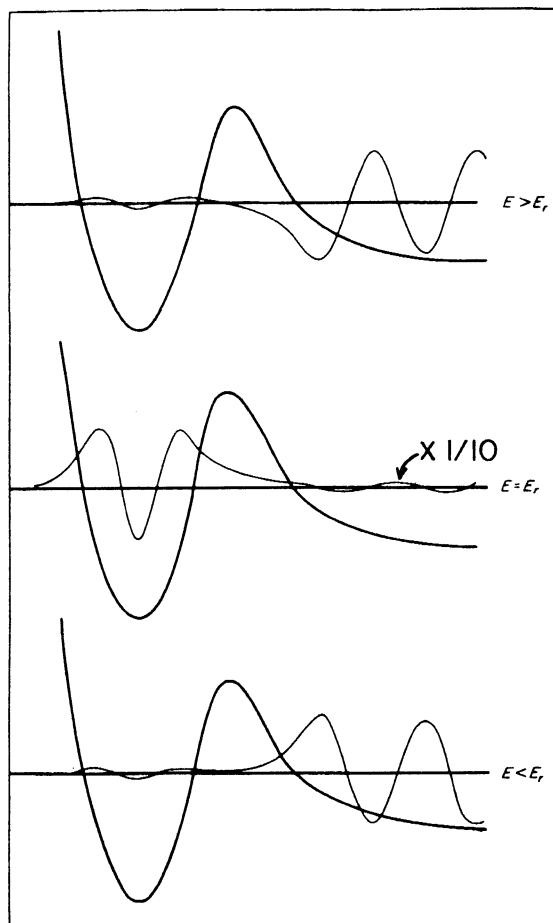


Fig. 2. Schematic of the effect of a potential barrier on an unbound wave function in the vicinity of a quasibound state at  $E = E_r$  (adapted from Ref. 20). In the present context, the horizontal axis represents the distance of the excited electron from the center of the molecule.

particular ionization channels and restrict motion only in certain directions. Again, a specific example is described below.

Focusing now on the wave functions in Fig. 2, we see the effect of the potential barrier on the wave mechanics of the photoelectron. For energies below the resonance energy  $E < E_r$  (lower part of Fig. 2), the inner well does not support a quasibound state, i.e., the wave function is not exponentially decaying as it enters the classically forbidden region of the barrier. Thus the wave function begins to diverge in the barrier region and emerges in the outer well with a much larger amplitude than that in the inner well. When properly normalized at large  $r$ , the amplitude in the molecular core is very small, so we say this wave function is essentially an eigenfunction of the outer well although small precursor loops extend inside the barrier into the molecular core.

At  $E = E_r$ , the inner well supports a quasibound state. The wavefunction exhibits exponential decay in the barrier region so that, if

the barrier extended to  $r \rightarrow \infty$ , a true bound state would lie very near this total energy. Therefore, the antinode that was not supported in the inner well at  $E < E_r$  has traversed the barrier to become part of a quasibound wave form which decays monotonically until it reemerges in the outer-well region, much diminished in amplitude. This "barrier penetration" by an antinode produces a rapid increase in the asymptotic phase shift by  $\sim \pi$  radians and greatly enhances the amplitude in the inner well over a narrow band of energy near  $E_r$ . Therefore, at  $E = E_r$ , the wavefunction is essentially an eigenfunction of the inner well, although it decays through the barrier and reemerges in the outer well. The energy halfwidth of the resonance is related to the lifetime of the quasibound state and to the energy derivative of the rise in the phase shift in well-known ways. Finally, for  $E > E_r$ , the wavefunction reverts to being an eigenfunction of the outer well as the behavior of the wavefunction at the outer edge of the inner well is no longer characteristic of a bound state.

Obviously this resonant behavior will cause significant physical effects: The enhancement of the inner-well amplitude at  $E \sim E_r$  results in good overlap with the initial states which reside mainly in the inner well. Conversely, for energies below the top of the barrier, but not within the resonance halfwidth of  $E_r$ , the inner amplitude is diminished relative to a more typical barrier-free case. This accounts for the strong modulation of the oscillator strength distribution in Fig. 1. Also, the rapid rise in the phase shift induces shape resonance effects in the photoelectron angular distribution. Another important aspect is that eigenfunctions of the inner well are localized inside the barrier and are substantially uncoupled from the external environment of the molecule. As mentioned above, this means that shape resonant phenomena often persist in going from the gas phase to the condensed phase, e.g., Fig. 1, and, with suitable modification, shape resonances in molecular photoionization can be mapped<sup>22</sup> onto electron-scattering processes and vice versa. Finally, note that this discussion was focussed on total energies from the bottom of the outer well to the top of the barrier, and that no explicit mention was made of the asymptotic potential that determines the threshold for ionization. Thus, valence or Rydberg states in this range can also exhibit shape resonant enhancement, even though they have true bound state behavior at large  $r$ , beyond the outer well.

We will now turn, for the remainder of this section, to the specific example of the well-known  $\sigma_u$  shape resonance in  $N_2$  photoionization, which was the first documented case<sup>23</sup> in a diatomic molecule and has since been used as a prototype in studies of various shape resonance effects, as discussed below. To identify the major final-state features in  $N_2$  photoionization at the independent-electron level, we show in Fig. 3 the original calculation<sup>23-25</sup> of the K-shell photoionization spectrum performed with the multiple-scattering model. This calculation agrees qualitatively with all major features in the experimental spectrum,<sup>26,27</sup> except a narrow band of double excitation features, and with subsequent, more accurate calculations.<sup>2,28</sup> The four partial cross sections in Fig. 3 represent the four dipole-allowed channels for K-shell (IP = 409.9 eV) photoionization. Here we have neglected the localization<sup>29</sup> of the K-shell hole since it doesn't greatly affect the integrated cross section and since the separation into u and g symmetry both helps the present discussion and is rigorously applicable to the subsequent discussion of valence-shell excitation. (Note that the identification of shape resonant behavior is generally easier in inner-shell spectra since the problems of overlapping spectra, channel interaction, and zeros in the dipole matrix element are reduced relative to valence-shell spectra.)

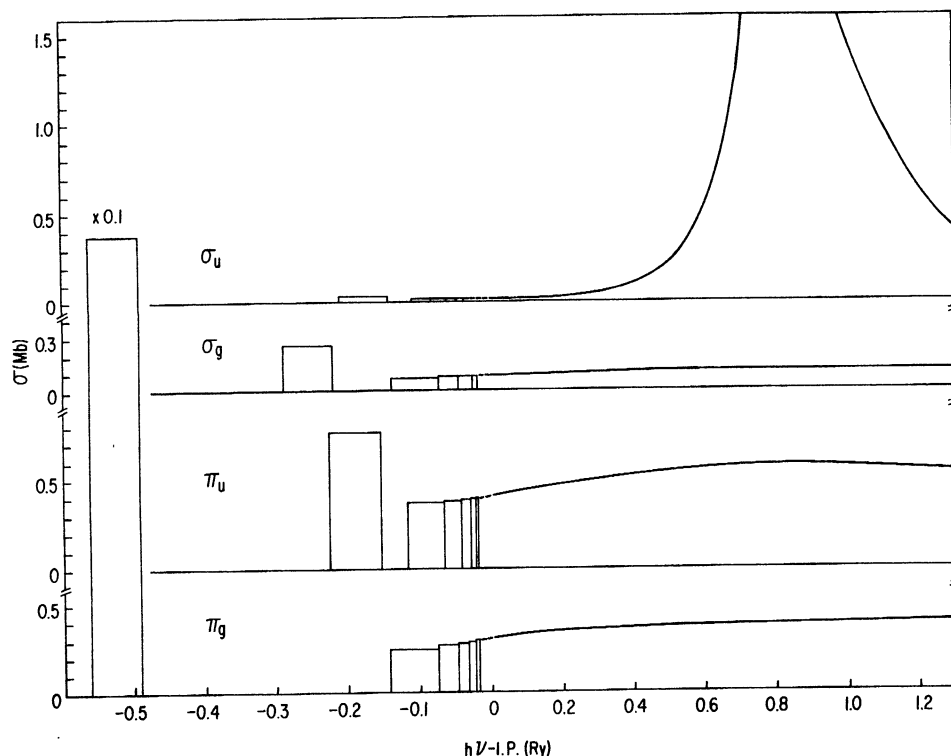


Fig. 3. Partial photoionization cross sections for the four dipole-allowed channels in K-shell photoionization of  $N_2$ . Note that the energy scale is referenced to the K-shell IP (409.9 eV) and is expanded two-fold in the discrete part of the spectrum.

The most striking spectral feature in Fig. 3 is the first member of the  $\pi_g$  sequence, which dominates every other feature in the theoretical spectrum by a factor of  $\sim 30$ . (Note the first  $\pi_g$  peak has been reduced by a factor of 10 to fit in the frame.) The concentration of oscillator strength in this peak is a centrifugal barrier effect in the d-wave component of the  $\pi_g$  wave-function. The final state in this transition is a highly localized state, about the size of the molecular core, and is the counterpart of the well-known<sup>3,19</sup>  $\pi_g$  shape resonance in  $e-N_2$  scattering at 2.4 eV. For the latter case, Krauss and Mies<sup>30</sup> demonstrated that the effective potential for the  $\pi_g$  elastic channel in  $e-N_2$  scattering exhibits a potential barrier due to the centrifugal repulsion acting on the dominant  $\ell = 2$  lead term in the partial-wave expansion of the  $\pi_g$  wavefunction. In the case of  $N_2$  photoionization, there is one less electron in the molecular field to screen the nuclear charge so that this resonance feature is shifted<sup>22</sup> to lower energy and appears in the discrete. It is in this sense that we refer to such features as "discrete" shape resonances. The remainder of the  $\pi_g$  partial cross section consists of a Rydberg series and a flat continuum. The  $\pi_u$  and  $\sigma_g$  channels both exhibit Rydberg series, the initial members of which correlate well with partially resolved transitions in the experimental spectrum below the K-shell IP.

The  $\sigma_u$  partial cross section, on the other hand, was found to exhibit behavior rather unexpected for the K shell of a first-row diatomic. Its Rydberg series was extremely weak, and an intense, broad peak appeared at  $\sim 1$  Ry above the IP in the low-energy continuum. This effect is caused by a centrifugal barrier acting on the  $\ell = 3$  component of the  $\sigma_u$  wavefunction. The essence of the phenomena can be described in mechanistic terms as follows. The electric dipole interaction, localized within the atomic K shell, produces a photoelectron with angular momentum  $\ell = 1$ . As this p-wave electron escapes to infinity, the anisotropic molecular field can scatter it into the entire range of angular momentum states contributing to the allowed  $\sigma$ - and  $\pi$ - ionization channels ( $\Delta\lambda = 0, \pm 1$ ). In addition, the spatial extent of the molecular field, consisting of two atoms separated by 1.1 Å, enables the  $\ell = 3$  component of the  $\sigma_u$  continuum wavefunction to overcome its centrifugal barrier and penetrate into the molecular core at a kinetic energy of  $\sim 1$  Ry. This penetration is rapid,<sup>23</sup> a phase shift of  $\sim \pi$  occurring over a range of  $\sim 0.3$  Ry. These two circumstances combine to produce a dramatic enhancement of photocurrent at  $\sim 1$  Ry kinetic energy, with predominantly f-wave character.

The specifically molecular character of this phenomenon is emphasized by comparison with K-shell photoionization in atomic nitrogen and in the united-atom case, silicon. In contrast to  $N_2$ , there is no mechanism for the essential p-f coupling, and neither atomic field is strong enough to support resonant penetration of high- $\ell$  partial waves through their centrifugal barriers. (With substitution of "d" for "f," this argument applies equally well to the d-type resonance in the discrete part of the spectrum.) Note that the  $\pi_u$  channel also has an  $\ell = 3$  component but does not resonate. This underscores the directionality and symmetry dependence of the trapping mechanism.

To place the  $\sigma_u$  resonance in a broader perspective and show its connection with high-energy behavior, we show, in Fig. 4, an extension of the calculation in Fig. 3 to much higher energy. Again the four dipole-allowed channels in  $D_{\infty h}$  symmetry are shown. The dashed line is two times the atomic nitrogen K-shell cross section. Note that the modulation about the atomic cross section, caused by the potential barrier, extends to  $\sim 100$  eV above threshold before the molecular and atomic curves seem to coalesce.

At higher energies, a weaker modulation appears in each partial cross section. This weak modulation is a diffraction pattern, resulting from scattering of the photoelectron by the neighboring atom in the molecule, or, more precisely, by the molecular field. Structure of this type was first studied over 50 years ago by de Kronig<sup>31</sup> in the context of metal lattices. It currently goes by the acronym EXAFS (extended x-ray absorption fine structure) and is used extensively<sup>32,33</sup> for local structure determination in molecules, solids, and surfaces. The net oscillation is very weak in  $N_2$ , since the light atom is a weak scatterer. More pronounced effects are seen, e.g., in K-shell spectra<sup>34</sup> of  $Br_2$  and  $GeCl_4$ . Our reason for showing the weak EXAFS structure in  $N_2$  is to show that the low-energy, resonant modulation (called "near-edge" structure in the context of EXAFS) and high-energy EXAFS evolve continuously into one another and emerge naturally from a single molecular framework, although the latter is usually treated from an atomic point-of-view.

Figure 5 shows a hypothetical experiment<sup>24</sup> which clearly demonstrates the  $\ell$  character of the  $\sigma_u$  resonance. In this experiment, we first fix the nitrogen molecule in space and orient the polarization direction of a photon beam, tuned near the nitrogen K edge, along the

molecular axis. This orientation will cause photoexcitation into  $\sigma$  final states, including the resonant  $\sigma_u$  ionization channel. (Again hole localization is neglected for purposes of illustration.) Figure 5 shows the angular distribution of photocurrent as a function of both excess energy above the K-shell IP and angle of ejection,  $\theta$ , relative to the molecular axis. Very apparent in Fig. 5 is the enhanced photocurrent at the resonance position,  $KE \sim 1$  Ry. Moreover, the angular distribution exhibits three nodes, with most of the photocurrent exiting the molecule along the molecular axis and none at right angles to it. This is an f-wave ( $l = 3$ ) pattern and indicates clearly that the resonant enhancement is caused by an  $l = 3$  centrifugal barrier in the  $\sigma_u$  continuum of  $N_2$ . Thus, the centrifugal barrier has observable physical meaning and is not merely a theoretical construct. Note that the correspondence between the dominant asymptotic partial wave and the trapping mechanism is not always

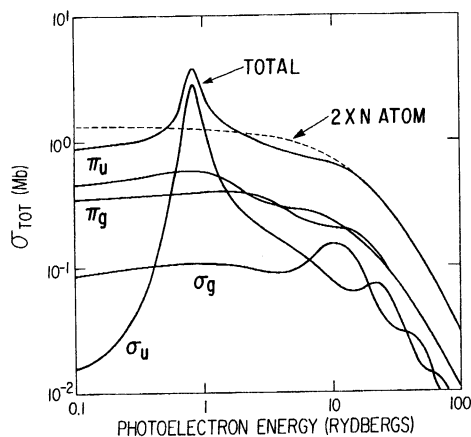


Fig. 4. Partial photoionization cross sections for the K shell of  $N_2$  over a broad energy range. The dashed line represents twice the K-shell photoionization cross section for atomic nitrogen, as represented by a Hartree-Slater potential.

valid, especially when the trapping is on an internal or off-center atomic site where the trapped partial wave can be scattered by the anisotropic molecular field into alternative asymptotic partial waves, e.g.,  $BF_3$ <sup>35</sup> and  $SF_6$ . Finally, note that the hypothetical experiment discussed above has been approximately realized by photoionizing molecules adsorbed on surfaces. The shape resonant features tend to survive adsorption and, owing to their observable  $l$ -character, can even provide evidence<sup>36,37</sup> as to the orientation of the molecule on the surface.

The final topic in the discussion of basic properties of shape resonances involves eigenchannel contour maps,<sup>38</sup> or, "pictures" of unbound electrons. This is the continuum counterpart of contour maps of bound-state electronic wavefunctions which have proven so valuable as

tools of quantum chemical visualization and analysis. Indeed, the present example helps achieve a physical picture of the  $\sigma_u$  shape resonance, and the general technique promises to be a useful tool for analyzing resonant trapping mechanisms and other observable properties in the future. The key to this visualization is the construction of those particular combinations of continuum orbital momenta that diagonalize the interaction of the unbound electron with the anisotropic molecular field. These combinations, known as eigenchannels, are the continuum analogues of the eigenstates in the discrete spectrum, i.e., the bound states.

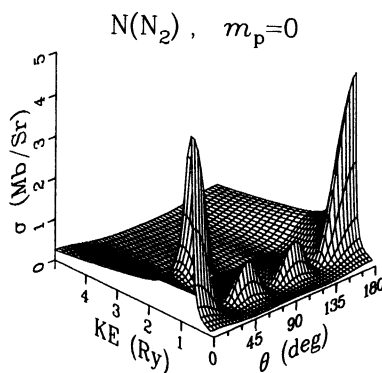


Fig. 5. Fixed-molecule photoelectron angular distribution for kinetic energies 0-5 Ry above the K-shell IP of  $N_2$ . The polarization of the ionizing radiation is oriented along the molecular axis in order to excite the  $\sigma$  continua, and the photoelectron ejection angle,  $\theta$ , is measured relative to the molecular axis.

The f-dominated eigenchannel of  $\sigma_u$  symmetry in  $N_2$  is an excellent case for which eigenchannel contour maps may be used to visualize shape resonant continuum states. In Fig. 6, this eigenchannel is plotted at two energies, one below the resonance energy and the other near the center of the resonance. In Fig. 6, the surfaces, whose contours have at large distance the three nodal planes characteristic of f orbitals, show clearly the resonant nature of the f-dominated  $\sigma_u$  eigenchannel. Below and above (not shown) the resonance energy, the probability amplitude and

its distribution inside and outside the molecular core is typical of non-resonant behavior. But at the resonance energy there is an enormous enhancement of the wavefunction in the molecular interior; the wavefunction now resembles a molecular bound-state probability amplitude distribution. It is this enhancement, in the region occupied by the bound states, that leads to the very large increase in oscillator strength indicative of the resonance, and to the other manifestations

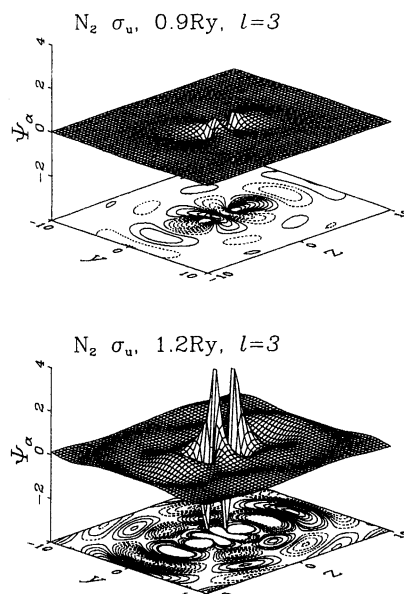


Fig. 6. F-wave-dominated eigenchannel wavefunctions for non-resonant (top) and resonant (bottom) electron kinetic energies in the  $\sigma_u$  continuum of  $N_2$ . The molecule is in the  $yz$  plane, along the  $z$  axis, centered at  $y = z = 0$ . Contours mark steps of 0.03 from 0.02 to 0.29; positive = solid, negative = dashed. The lack of contour lines for 1.2 Ry near the nuclei is because of the 0.29 cutoff.

discussed earlier and in the next section.

These eigenchannel plots are discussed more fully elsewhere;<sup>38</sup> however, before leaving the subject, several points should be noted. First, the  $N_2$  example that we have chosen is somewhat special in that there is a near one-to-one correspondence between the eigenchannels and single values of orbital angular momentum. Orbital angular momentum is, however, not a good quantum number in molecules, and more generally we

should not always expect such clear nodal patterns. More typically, earlier work<sup>5,35,39-41</sup> indicates that several angular momenta often contribute to the continuum eigenchannels (although a barrier in only one  $l$  component will be primarily responsible for the temporary trapping that causes the enhancement in that and coupled components), and this means that the resulting eigenchannel plots will be correspondingly richer. Second, the dominant  $l$  we have discussed pertains to the region outside the molecular charge distributions. The orbital momentum composition of these wavefunctions is more complicated in the molecular interior, as seen, e.g., in Fig. 6. Nonetheless, continuity and a dominant  $l$  may, as in the case of  $N_2$ , cause the emergence of a distinct  $l$  pattern, even into the core region. Third, while these ideas were developed<sup>38</sup> in the context of molecular photoionization, the continuum eigenchannel concept carries over without any fundamental change to electron-molecule scattering. Finally, while we have used one-electron wavefunctions here, obtained with the multiple-scattering model, we emphasize that the eigenchannel concept is a general one and we look forward to its use in the analysis of more sophisticated, many-electron molecular continuum wavefunctions.

#### IV. SHAPE-RESONANCE-INDUCED NON-FRANCK-CONDON EFFECTS

Molecular photoionization at wavelengths unaffected by autoionization, predissociation, or ionic thresholds was generally believed to produce Franck-Condon (FC) vibrational intensity distributions within the final ionic state and  $v$ -independent photoelectron angular distributions. We now discuss a prediction<sup>42,43</sup> from a few years ago, that shape resonances represent an important class of exceptions to this picture. These ideas are illustrated with a calculation of the  $3\sigma_g \rightarrow \epsilon\sigma_u, \epsilon\pi_u$  photoionization channel of  $N_2$ , which accesses the same  $\sigma_u^g$  shape resonance discussed above at approximately  $h\nu \sim 30$  eV, or  $\sim 14$  eV above the  $3\sigma_g$  IP. The process we are considering involves photoexcitation of  $N_2$   $X^1\Sigma_g^+$  in its vibrational ground state with photon energies from the first IP  $\epsilon_0$  beyond the region of the shape resonance at  $h\nu \sim 30$  eV. This process ejects photoelectrons leaving behind  $N_2^+$  ions in energetically accessible states. As we are interested in the ionization of the  $3\sigma_g$  electron, which produces the  $X^2\Sigma_g^+$  ground state of  $N_2^+$ , we are concerned with the photoelectron band in the range  $15.5 \text{ eV} < \text{IP} < 16.5 \text{ eV}$ . The physical effects we seek involve the relative intensities and angular distributions of the  $v = 0-2$  vibrational peaks in the  $X^2\Sigma_g^+$  electronic band, and, more specifically, the departures of these observables from behavior predicted by the FC separation.

The breakdown of the FC principle arises from the quasibound nature of the shape resonance, which, as we discussed in Section III, is localized in a spatial region of molecular dimensions by a centrifugal barrier. This barrier and, hence, the energy and lifetime (width) of the resonance are sensitive functions of internuclear separation  $R$  and vary significantly over a range of  $R$  corresponding to the ground-state vibrational motion. This is illustrated in the upper portion of Fig. 7 where the dashed curves represent separate, fixed- $R$  calculations of the partial cross section for  $N_2$   $3\sigma_g$  photoionization over the range  $1.824a_0 < R < 2.324a_0$ , which spans the  $N_2$  ground-state vibrational wavefunction.

Of central importance in Fig. 7 is the clear demonstration that resonance positions, strengths, and widths are sensitive functions of  $R$ . In particular, for larger separations, the inner well of the effective potential acting on the  $l = 3$  component of the  $\sigma_u$  wavefunction is more attractive and the shape resonance shifts to lower kinetic energy, becoming narrower and higher. Conversely, for lower values of  $R$ ,

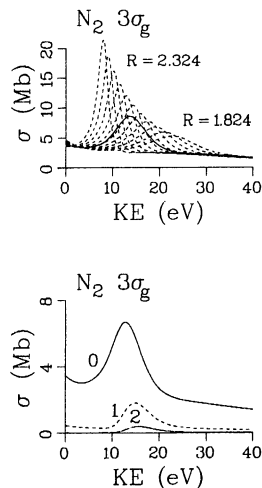


Fig. 7. Cross sections  $\sigma$  for photoionization of the  $3\sigma_g$  ( $v_i = 0$ ) level of  $N_2$ . Top: fixed- $R$  (dashed curves) and  $R$ -averaged, vibrationally unresolved (solid curve) results. Bottom: results for resolved final-state vibrational levels,  $v_f = 0 - 2$ .

the resonance is pushed to higher kinetic energy and is weakened. This indicates that nuclear motion exercises great leverage on the spectral behavior of shape resonances, since small variations in  $R$  can significantly shift the delicate balance between attractive (mainly Coulomb) and repulsive (mainly centrifugal) forces which combine to form the barrier. In the present case, variations in  $R$ , corresponding to the ground-state vibration in  $N_2$ , produce significant shifts of the resonant behavior over a spectral range several times the fullwidth at half maximum of the resonance calculated at  $R = R_e$ . By contrast, nonresonant channels are relatively insensitive to such variation in  $R$ , as was shown by results<sup>44</sup> on the  $1\pi_u$  and  $2\sigma_u$  photoionization channels in  $N_2$ .

Thus, in the vicinity of a shape resonance, the electronic transition moment varies rapidly with  $R$ . This parametric coupling was estimated<sup>42</sup> in the adiabatic-nuclei approximation<sup>45</sup> by computing the net transition moment for a particular vibrational channel as an average of the  $R$ -dependent dipole amplitude, weighted by the product of the initial-

and final-state vibrational wavefunctions at each R,

$$D_{v_f v_i} = \int dR \chi_{v_f}^\dagger(R) D^-(R) \chi_{v_i}(R).$$

The vibrational wavefunctions were approximated by harmonic-oscillator functions and the superscript minus denotes that incoming-wave boundary conditions have been applied and that the transition moment is complex. Note that, even when the final vibrational levels  $v_f$  of the ion are unresolved (summed over), vibrational motion within the initial state  $v_i = 0$  can cause the above equation to yield results significantly different from the  $R = R_e$  result, because the R dependence of the shape resonance is highly asymmetric. This gross effect of R averaging can be seen in the upper half of Fig. 7 by comparing the solid line (R-averaged result, summed over  $v_f$ ) and the middle dashed line ( $R = R_e$ ). Hence, even for the calculation of gross properties of the whole, unresolved electron band, it is necessary to take into account vibrational-motion effects in channels exhibiting shape resonances. As we stated earlier, this is generally not a critical issue in nonresonant channels.

Effects of nuclear motion on individual vibrational levels are shown in the bottom half of Fig. 7. Looking at the partial cross sections in Fig. 7, we see that the resonance position varies over a few volts depending on the final vibrational state, and that higher levels are relatively more enhanced at their resonance position than is  $v_f = 0$ . This sensitivity to  $v_f$  arises because transitions to alternative final vibrational states preferentially sample different regions of R. In particular,  $v_f = 1, 2$  sample successively smaller R, governed by the maximum overlap with the ground vibrational state, causing the resonance in those vibrational channels to peak at higher energy than that for  $v_f = 0$ . The impact of these effects on branching ratios is clearly seen in Fig. 2 of Ref. 42, where the ratio of the higher  $v_f$  intensities to that of  $v_f = 0$  is plotted in the resonance region. There we see that the ratios are slightly above the FC factors (9.3%,  $v_f = 1$ ; 0.6%,  $v_f = 2$ ) at zero kinetic energy, go through a minimum just below the resonance energy in  $v_f = 0$ , then increase to a maximum as individual  $v_f > 0$  vibrational intensities peak, and finally approach the FC factors again at high kinetic energy. Note the maximum enhancement over the FC factors is progressively more pronounced for higher  $v_f$ , i.e., 340% and 1300% for  $v_f = 1, 2$ , respectively.

Equally dramatic are the effects on  $\beta(v_f)$  discussed in Ref. 42. Especially at and below the resonance position, the  $\beta$ 's vary greatly for different final vibrational levels. Carlson first observed<sup>46,47</sup> that, at 584 Å, the  $v_f = 1$  level in the  $3\sigma_g$  channel of  $N_2$  had a much larger  $\beta$  than the  $v_f = 0$  level even though there was no apparent autoionizing state at that wavelength. This is in semiquantitative agreement with the theoretical calculation<sup>42</sup> which gives  $\beta(v_f = 0) \sim 1.0$  and  $\beta(v_f = 1) \sim 1.5$ . Although the agreement is not exact, we feel this demonstrates that the "anomalous"  $v_f$  dependence of  $\beta$  in  $N_2$  stems mainly from the  $\sigma_u$  shape resonance which acts over a range of the spectrum many times its own  $\sim 5$  eV width. The underlying cause of this effect is the shape-resonance-enhanced R dependence of the dipole amplitude, just as for the vibrational partial cross sections. In the case of  $\beta(v_f)$ , however, both the R dependence of the phase and of the magnitude of the complex dipole amplitude play a crucial role, whereas the partial cross sections depend only on the magnitude.

The theoretical predictions discussed above were soon tested in two separate experiments. In Fig. 8 the branching ratio for production of the  $v = 0$  and 1 vibrational levels of  $N_2^+ X^2\Sigma_g^+$  is shown. The dash-dot line is the original prediction.<sup>42</sup> The solid dots are the recent

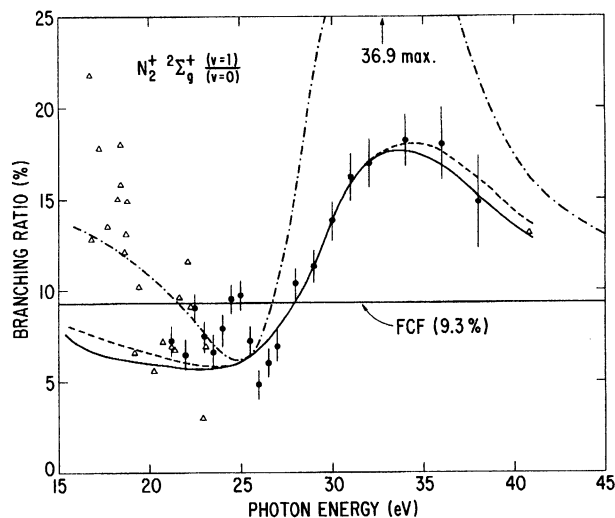


Fig. 8. Branching ratios for production of the  $v = 0, 1$  levels of  $N_2^+ X^2\Sigma_g^+$  by photoionization of  $N_2$ : ●, Ref. 48; Δ, Ref. 49; -·-·-, multiple scattering model prediction from Ref. 42; —, frozen-core Hartree-Fock dipole length approximation from Ref. 50; - - -, frozen-core Hartree-Fock dipole velocity approximation from Ref. 50.

measurements<sup>48</sup> in the vicinity of the shape resonance at  $h\nu \sim 30$  eV. The conclusion drawn from this comparison is that the observed variation of the vibrational branching ratio relative to the FC factor over a broad spectral range qualitatively confirms the prediction; however, subsequent calculations<sup>7,50</sup> with fewer approximations have achieved better agreement based on the same mechanism for breakdown of the FC separation. The dashed and solid curves are results based on a Schwinger variational treatment<sup>50</sup> of the photoelectron wavefunction. The two curves represent a length and velocity representation of the transition matrix element, both of which are in excellent agreement with the data. This is an outstanding example of interaction between experiment and theory, proceeding as it did from a novel prediction, through experimental testing and final quantitative theoretical agreement in a short time. Also shown in Fig. 8 are data in the  $15.5 \text{ eV} < h\nu < 22 \text{ eV}$  region which are earlier data<sup>49</sup> obtained using laboratory line sources. The apparently chaotic behavior arises from unresolved autoionization structure.

The angular distribution asymmetry parameters,  $\beta$ , for the  $v = 0, 1$  levels of  $N_2^+ X^2\Sigma_g^+$  over roughly the same energy region are reported in Ref. 51. In the region above  $h\nu \sim 25$  eV, this data also shows

qualitative agreement with the predicted<sup>42</sup>  $v$ -dependence of  $\beta$  caused by the  $\sigma_u$  shape resonance.<sup>50</sup> In this case, the agreement is somewhat improved in later calculations,<sup>50</sup> mainly for  $v = 1$ ; however, the change is less dramatic than for the branching ratios.

Finally, note that we have illustrated the vibrational effects of shape resonances in the context of molecular photoionization; however, a rather analogous mechanism makes shape resonances extremely efficient in inducing vibrational excitation in electronically-elastic electron-molecule scattering.<sup>3,19,43</sup>

#### V. CONNECTIONS BETWEEN SHAPE RESONANCES IN ELECTRON-MOLECULE SCATTERING AND IN MOLECULAR PHOTOIONIZATION AND RELATED CONNECTIONS

At first glance, there is little connection between resonances in electron-molecule scattering ( $e + M$ ) and those in molecular photoionization ( $h\nu + M$ ). The two phenomena involve different numbers of electrons and the collision velocities are such that all electrons are incorporated into a collision complex. Hence, we are comparing a neutral molecule to a molecular negative-ion system. However, although the long-range part of the scattering potential is drastically different in the two cases, the inner part is not drastically different since it is dominated by the interactions among the nuclei and those electrons common to both systems. Thus, shape resonances which are localized in the molecular core substantially maintain their identity from one system to another, but are shifted in energy owing to the difference caused by the addition of an electron inside the molecule. This unifying property of shape resonances thus links together the two largest bodies of data for the molecular continuum --  $h\nu + M$  and  $e + M$  -- and, although these resonances shift in energy in going from one class to another and manifest themselves in somewhat different ways, this link permits us to transfer information between the two. This can serve to help interpret new data and even to make predictions of new features to look for experimentally. Actually, this picture<sup>22</sup> was surmised empirically from evidence contained in survey calculations on  $e + M$  and  $h\nu + M$  and, in retrospect, from data. These observations can be summarized as follows: By and large, the systems  $h\nu + M$  and  $e + M$  display the same manifold of shape resonances, only those in the  $e + M$  system are shifted  $\sim 10$  eV to higher electron energy. Usually, there is one shape resonance per symmetry for a subset of the symmetries available. The shift depends on the symmetry of the state, indicating, as one would expect, that the additional electron is not uniformly distributed. Finally, there is substantial proof that the  $\ell$  character is preserved in this process, although interaction among alternative components in a scattering eigenchannel can alter the  $\ell$  mixing present.

There are several good examples available to illustrate this point, e.g.,  $N_2$ ,  $CO$ ,  $CO_2$ ,  $BF_3$ ,  $SF_6$ , etc. In general, one can start from either the neutral or the negative ion system, but, in either case, there is a preferred way to do so: In the  $h\nu + M$  case, it is better to examine the inner-shell photoabsorption and photoionization spectra. Shape resonances almost invariably emerge most clearly in this context. Additional effects, discussed briefly at the end of this section, frequently make the role of shape resonances in valence-shell spectra more complicated to interpret. In the  $e + M$  case, a very sensitive indicator of shape resonance behavior is the vibrational excitation channel. Vibrational excitation is enhanced by shape resonances,<sup>3,19</sup> and is typically very weak for non-resonant scattering. Hence, a shape resonance, particularly at intermediate energy (10-40 eV),<sup>43,52</sup> may be barely visible in the vibrationally and electronically elastic scattering

cross section, and yet be displayed prominently in the vibrationally inelastic, electronically elastic cross section.

Two examples will help illustrate these points. In  $e - SF_6$  scattering, the vibrationally elastic scattering cross section has been calculated theoretically<sup>53</sup> and shown to have four shape resonances of  $a_{1g}$ ,  $t_{1u}$ ,  $t_{2g}$ , and  $e_g$  symmetry at approximately 2, 7, 13, and 27 eV, respectively. The absolute total cross section measured by Kennerly et al.<sup>54</sup> shows qualitative agreement, except that no clear sign of the  $e_g$  is present. (This resonance could be more clearly seen in the vibrational excitation spectrum, which is not available.) Hence, using the guidelines given above, one would expect shape resonance features in the  $h\nu + M$  case at -8, -3, 3, and 17 eV (on the kinetic energy scale) to a very crude, first approximation. Indeed, the K- and L-shell photoabsorption spectra of  $SF_6$  show such intense features, as discussed in Section II.

Using  $N_2$ , we reverse the direction of the mapping, and start with  $h\nu + N_2$ , which was discussed extensively in earlier sections. Here a "discrete" shape resonance of  $\pi_g$  symmetry and a shape resonance of  $\sigma_u$  symmetry are apparent in the K-shell spectrum,<sup>26</sup> e.g., Fig. 3. These occur at  $\sim -9$  and 10 eV on the kinetic energy scale (relative to the ionization potential). Hence, one would look for the same set of resonances in  $e-N_2$  scattering at  $\sim 1$  and  $\sim 20$  eV electron scattering energies. The well-known  $\pi_g$  shape resonance<sup>19</sup> is very apparent in the vibrationally elastic cross section; however, there is only a very broad bump at  $\sim 20$  eV.<sup>55</sup> As noted above, the vibrationally inelastic cross section is much more sensitive to shape resonances, and, indeed, the  $\sigma_u$  shape resonance in  $e-N_2$  scattering has been established theoretically and experimentally by looking in this channel (see e.g., Refs. 43, 56-60). Several other excellent examples exist, but we will conclude by pointing out that the connections between  $e-CO_2$  and  $h\nu - CO_2$  have been recently discussed<sup>41</sup> in detail, including a study of the eigenphase sums in the vicinity of the  $\sigma_u$  shape resonance in the two systems.

Finally, we note similar connections and additional complications upon mapping from inner-shell to valence-shell  $h\nu + M$  spectra. On going from deep inner-shell spectra to valence-shell spectra, shape resonances in  $h\nu + M$  also shift approximately 1-4 eV toward higher kinetic energy, due to differences in screening between localized and delocalized holes as well as other factors. As mentioned above, several complications arise in valence-shell spectra which can tend to obscure the presence of a shape resonance compared to their more straightforward role in inner-shell spectra. These include greater energy dependence of the dipole matrix element, interactions with autoionizing levels, strong continuum-continuum coupling between more nearly degenerate ionization channels, strong particle-hole interactions, etc. So, for the most transparent view of the manifold of shape resonance features in  $h\nu + M$ , one should always begin with inner-shell photoabsorption data.

## VI. PROGRESS AND PROSPECTS

Summarizing, we have used prototype studies on  $N_2$  to convey the progress made in the study of shape resonances in molecular fields, particularly in molecular photoionization. This included the identification of shape resonant features in photoionization spectra of molecules and the accrual of substantial physical insight into their properties, many of which were peculiar to molecular fields. One recent example has been the prediction and experimental confirmation of the role of shape resonances in producing non-Franck-Condon effects in vibrational

branching ratios and photoelectron angular distribution.

What this discussion has failed so far to convey is the already extensive body of work that has developed around these basic themes. Even in an early interpretation<sup>18</sup> of shape resonance effects in x-ray spectra, it was obvious that the phenomena would be widespread as over ten molecules, or local molecular moieties, were already observed (see, e.g., Refs. 15 and 18) to have shape resonant behavior. At the present, it is not difficult to identify over two dozen examples of molecules exhibiting the effects discussed above in one or more final state symmetries (references for the following examples are cited in Ref. 1, and the inner-shell cases are listed according to molecule in the bibliography given by Hitchcock<sup>61</sup>). These include simple diatomics ( $N_2$ ,  $O_2$ , CO, NO), polyatomics with subgroups related to the first-row diatomics (HCN,  $C_2N_2$ ,  $CH_3CH$ ), triatomics ( $CO_2$ ,  $CS_2$ , OCS,  $N_2O$ ,  $SO_2$ ) and more highly coordinated molecules and local molecular environments ( $SF_6$ ,  $SO_4$ ,  $SF_5CF_3$ ,  $SF_2O_2$ ,  $SF_2O$ ,  $BF_3$ ,  $SiF_4$ ,  $SiCl_4$ ,  $SiF_6$ ,  $SiO_2$ ,  $NF_3$ ,  $CF_4$ ). There is no doubt that many cases have been overlooked in this list and that many examples will be identified in the future as the exploration of molecular photoionization dynamics continues, particularly with the increasing utilization of synchrotron radiation sources.

Several examples from this body of literature serve both to emphasize some of the interesting complications that can arise and to caution against assuming that manifestations of shape resonances will always conform to the independent-electron concepts used above to explain the fundamentals of the subject in connection with  $N_2$  photoionization: (i) One recently documented case of many-body interactions causing deviations from the single-channel picture stressed above is continuum-continuum coupling in the  $2\sigma_u^{-1}$  photoionization channel of  $N_2$ .<sup>62-66</sup> In the single-channel model, the  $\sigma_u$  shape resonance would not affect this channel; however, channel interaction between the  $2\sigma_u^{-1}$  and  $3\sigma_g^{-1}$  ionization continua has been shown<sup>62</sup> to cause resonant structure in the  $\beta$  for the  $2\sigma_u^{-1}$  channel at the energy of the  $\sigma_u$  shape resonance in the  $3\sigma_g^{-1}$  channel. This mechanism had also been cited in the valence-shell photoionization of  $SF_6$ ,<sup>67</sup> and should be a general phenomenon. (ii) In the case of  $O_2$  photoionization, an analogous  $\sigma_u$  shape resonance is expected,<sup>68-70</sup> but its identification in the photoionization spectrum has been complicated by the existence of extensive autoionization structure in the region of interest. Recent work<sup>71</sup> using variable wavelength photoelectron measurements and a multichannel quantum defect theory (MQDT) analysis of the principal autoionizing Rydberg series has sorted out this puzzle, with the result that the  $\sigma_u$  shape resonance was established to be approximately where expected, but was not at all clearly identifiable without the extensive analysis used in this case. Several examples now exist which exhibit overlapping shape and autoionizing resonances, thus requiring great care in order to arrive at meaningful interpretation. This will be common, particularly in valence spectra where successive IP's are closely spaced. (iii) In the case of  $CO_2$  a  $\sigma_u$  shape resonance of completely different origin was expected<sup>39,72</sup> for photoionization of the  $4\sigma_g$  orbital, leading to the  $C\ 2\sigma_g^+$  state of  $CO_2^+$ . This resonance, however,<sup>73</sup> was not apparent in partial cross section measurements on this channel.<sup>73</sup> Nevertheless predictions<sup>40,72</sup> of a shape-resonant feature in the corresponding  $\beta$  was confirmed<sup>74</sup> and work in several laboratories<sup>39,40,72,74-80</sup> have now converged to reasonable agreement in this observable. In addition, recent measurements have shown that this resonance is observable in the partial cross sections, but is shifted to lower energy and much diminished.<sup>80</sup> Future experimental work on vibrational branching ratios and v-dependent  $\beta$ 's<sup>40</sup> would greatly aid in the further study of this case. Several other examples of shape resonances which are clearly displayed in some (usually inner-

shell) spectra, but are "missing" in other (usually valence-shell) spectra are now known.<sup>81-83</sup> One of the remaining intriguing problems is to pinpoint the key interaction which erases the shape resonance in certain channels. (iv) One of the exciting new results involves studying resonances in inner-shell spectra with electron spectroscopy.<sup>84,85</sup> This type of measurement goes beyond the absorption type measurement and gives information on the decay of resonant features. In fact many resonances in SF<sub>6</sub>, SiF<sub>4</sub>, and other molecules decay by barrier penetration into the direct ionization continuum of the main single-hole configuration; however, Ferrett et al.<sup>85</sup> have noted exceptions, such as the e<sub>g</sub> in SF<sub>6</sub> which decays with a finite branching ratio into satellite configurations. Hence, the enhanced excitation is caused by a simple shape resonant mechanism, but the decay involves multiparticle interactions, to a significant extent. Other observations include decay paths for discrete resonances excited from deep inner holes,<sup>84</sup> anisotropy,<sup>85</sup> or lack of it,<sup>84</sup> in Auger angular distributions following resonant excitation; and characterization of weak features in the K spectra of SF<sub>6</sub> as doubly excited states converging to satellite thresholds.<sup>84,85</sup> This is a rich and complicated stream of work, just getting underway. It is now feasible owing to developments in synchrotron radiation. (v) Returning to the case of N<sub>2</sub>, we note that the photoionization of the 2σ<sub>g</sub> should also access the σ<sub>u</sub> shape resonance. However, for this inner-valence orbital, extensive vibronic coupling leads to a breakdown<sup>86</sup> of the single-particle model leading to the observation<sup>87</sup> of many "satellite" vibronic states in the photoelectron spectrum instead of a single peak due to ionization of the 2σ<sub>g</sub> orbital. Nevertheless, if the sum of this complicated structure is plotted versus photon energy, the resonant enhancement reemerges.<sup>87,88</sup> (vi) Owing to the dependence of continuum resonances on internuclear separation, an examination of the utility of resonance positions in families of molecules to predict interatomic spacings was attempted.<sup>89</sup> Early results were very optimistic, claiming an accuracy of 0.05 Å; however, more conservative analyses<sup>90</sup> made it clear that, while the basic qualitative principal may be correct, the application to structure determination was not as promising as initially thought. (vii) Finally, in most molecules, a resonant channel will have only one resonance; however, in polyatomics, multiple resonances have been documented<sup>91</sup> in cases such as C<sub>2</sub>N<sub>2</sub>, where two resonances are found in the σ<sub>u</sub> channel, resulting from the trapping on the C-C and C-N sites. In addition, N<sub>2</sub>O exhibits<sup>92</sup> two resonances in the σ channel but without obvious correlation with different sites. In this case, two alternative ℓ's may resonate, or the higher energy feature could be the transition region between resonant trapping and diffractive scattering, where quantum mechanical ringing may be a more apt description. More detailed work is required to sort out this detail.

These eight cases are excellent examples of the additional types of challenges that can arise in the study of shape resonance phenomena. They should not diminish the simplicity and power of the fundamental shape resonance dynamics but, rather, should show how this fundamental framework showcases more complicated (and interesting) photoionization dynamics which, in turn, require a more sophisticated framework for full understanding.

Another form of progress is measured by the applicability of ideas to other observables, or, more broadly, to other subfields: (i) We have already touched upon the close connection<sup>22</sup> between shape resonance phenomena in molecular photoionization and electron-molecule scattering. (ii) Shape resonances in adsorbed molecules are now used rather extensively<sup>36,37</sup> as a probe of the geometry and electronic properties of adsorption sites. (iii) As discussed in connection with the inner-shell spectra of SF<sub>6</sub>, free-molecule concepts concerning

localized states carry over to the condensed phase. In such cases, a local "molecular" point-of-view can often provide more direct physical insight into photoexcitation dynamics of solids than can a band-structure approach. (iv) Also noted above, shape resonances are often low-energy precursors to EXAFS structure occurring from ~100 eV to thousands of eV above inner-shell edges. (v) An intimate connection also exists with antibonding valence states in quantum chemistry language.<sup>93</sup> This was dramatically demonstrated over ten years ago, when Gianturco et al.<sup>94</sup> interpreted the shape resonances in SF<sub>6</sub> using unoccupied virtual orbitals in an LCAO-MO calculation. This connection is a natural one since shape resonances are localized within the molecular charge distribution and therefore can be realistically described by a limited basis set suitable for describing the valence MO's. However, the scattering approach used in the shape-resonance picture is necessary for analysis of various dynamical aspects of the phenomena. (vi) Finally, shape resonances have been used as characteristic features in the analysis of such diverse subjects as electron optics<sup>5</sup> of molecular fields and hole localization<sup>29</sup> in inner-shell ionization, and as the cause for molecular alignment in photoionization, leading to anisotropy in the angular distribution<sup>95,96</sup> of Auger electrons from the decay of K-shell holes.

Clearly the subject of shape resonances in molecular fields has developed into a mature subfield. To a large extent the dynamics described above are now employed in a more or less routine fashion to interpret molecular photophysics and electron scattering processes. Nevertheless several challenges remain, mainly in the cases of significant departures from the simple concepts offered above. These will be due in large part to multiparticle mechanisms, such as those enumerated earlier in this section. Another interesting direction will be to study the effects of resonant excitations in more complicated vibrational modes and dissociative processes. In these and unforeseen ways, the expansion, refinement, and unification of ongoing developments in the study of shape resonances in molecular fields should remain an active theme in molecular physics in the coming years.

#### References

1. J. L. Dehmer, A. C. Parr, and S. H. Southworth, in: "Handbook on Synchrotron Radiation, Vol. II," ed. G. V. Marr, North Holland, Amsterdam (1987), p. 241 and references therein.
2. "Resonances in Electron-Molecule Scattering, van der Waals Complexes, and Reactive Chemical Dynamics," ACS Symposium Series, No. 263, ed. D. G. Truhlar, American Chemical Society, Washington, DC (1984).
3. N. F. Lane, Rev. Mod. Phys. 52:29 (1980), and references therein.
4. D. Dill and J. L. Dehmer, J. Chem. Phys. 61:692 (1974).
5. J. L. Dehmer and D. Dill, in: "Electron-Molecule and Photon-Molecule Collisions," eds. T. Rescigno, V. McKoy, and B. Schneider, Plenum, New York (1979), p. 225.
6. P. W. Langhoff, in: "Electron-Molecule and Photon-Molecule Collisions," eds. T. Rescigno, V. McKoy, and B. Schneider, Plenum, New York (1979), p. 183.
7. G. Raseev, H. Le Rouzo, and H. Lefebvre-Brion, J. Chem. Phys. 72:5701 (1980).
8. R. R. Lucchese and V. McKoy, Phys. Rev. A 24:770 (1981).
9. R. R. Lucchese, G. Raseev, and B. V. McKoy, Phys. Rev. A 25:2572 (1982).

10. Z. H. Levine and P. Soven, Phys. Rev. A 29:625 (1984).
11. L. A. Collins and B. I. Schneider, Phys. Rev. A 29:1695 (1984).
12. R. E. LaVilla and R. D. Deslattes, J. Chem. Phys. 44:4399 (1966).
13. R. E. LaVilla, J. Chem. Phys. 57:899 (1972).
14. T. M. Zimkina and V. A. Fomichev, Dokl. Akad. Nauk SSSR 169:1304 (1966) [Sov. Phys. Dokl. 11:726 (1966)].
15. T. M. Zimkina and A. C. Vinogradov, J. Phys. (Paris) Colloq. 32:3 (1971).
16. D. Blechschmidt, R. Haensel, E. E. Koch, U. Nielsen, and T. Sagawa, Chem. Phys. Lett. 14:33 (1972).
17. M. Nakamura, Y. Morioka, T. Hayaishi, E. Ishiguro, and M. Sasanuma, in: "Third International Conference on Vacuum Ultraviolet Radiation Physics," Physical Society of Japan, Tokyo (1971), paper IpA1-6.
18. J. L. Dehmer, J. Chem. Phys. 56:4496 (1972).
19. G. J. Schulz, Rev. Mod. Phys. 45:422 (1973).
20. M. S. Child, "Molecular Collision Theory," Academic, New York (1974), p. 51.
21. U. Fano and J. W. Cooper, Rev. Mod. Phys. 40:441 (1968).
22. J. L. Dehmer and D. Dill, in: "Symposium on Electron-Molecule Collisions," eds. I. Shimamura and M. Matsuzawa, University of Tokyo Press, Tokyo (1979), p. 95.
23. J. L. Dehmer and D. Dill, Phys. Rev. Lett. 35:213 (1975).
24. D. Dill, J. Siegel, and J. L. Dehmer, J. Chem. Phys. 65:3158 (1976).
25. J. L. Dehmer and D. Dill, J. Chem. Phys. 65:5327 (1976).
26. R. B. Kay, Ph. E. van der Leeuw, and M. J. van der Wiel, J. Phys. B 10:2513 (1977).
27. A. P. Hitchcock and C. E. Brion, J. Electron Spectrosc. 18:1 (1980).
28. T. N. Rescigno and P. W. Langhoff, Chem. Phys. Lett. 51:65 (1977).
29. D. Dill, S. Wallace, J. Siegel, and J. L. Dehmer, Phys. Rev. Lett. 41:1230 (1978); 42:411 (1979).
30. M. Krauss and F. H. Mies, Phys. Rev. A 1:1592 (1970).
31. R. L. de Kronig, Z. Physik 70:317 (1931); 75:191 (1932).
32. "Synchrotron Radiation: Techniques and Applications," ed. C. Kunz, Springer-Verlag, Berlin (1979).
33. "Synchrotron Radiation Research," eds. H. Winick and S. Doniach, Plenum, New York (1980).
34. B. Kincaid and P. Eisenberger, Phys. Rev. Lett. 34:1361 (1975).
35. J. R. Swanson, D. Dill, and J. L. Dehmer, J. Chem. Phys. 75:619 (1981).
36. T. Gustafsson, E. W. Plummer, and A. Liebsch, in: "Photoemission and the Electronic Properties of Surfaces," eds. B. Feuerbacher, B. Fitton, and R. F. Willis, J. Wiley, New York (1978).
37. T. Gustafsson, Surface Science 94:593 (1980).
38. D. Loomba, S. Wallace, D. Dill, and J. L. Dehmer, J. Chem. Phys. 75:4546 (1981).
39. J. R. Swanson, D. Dill, and J. L. Dehmer, J. Phys. B 13:L231 (1980).
40. J. R. Swanson, D. Dill, and J. L. Dehmer, J. Phys. B 14:L207 (1981).
41. P. M. Dittman, D. Dill, and J. L. Dehmer, Chem. Phys. 78:405 (1983).
42. J. L. Dehmer, D. Dill, and S. Wallace, Phys. Rev. Lett. 43:1005 (1979).
43. J. L. Dehmer and D. Dill, in: "Electronic and Atomic Collisions," eds. N. Oda and K. Takayanagi North-Holland, Amsterdam (1980), p. 195.
44. S. Wallace, Ph.D. thesis, Boston University (1980).
45. D. M. Chase, Phys. Rev. 104:838 (1956).
46. T. A. Carlson, Chem. Phys. Lett. 9:23 (1971).
47. T. A. Carlson and A. E. Jonas, J. Chem. Phys. 55:4913 (1971).
48. J. B. West, A. C. Parr, B. E. Cole, D. L. Ederer, R. Stockbauer, and J. L. Dehmer, J. Phys. B 13:L105 (1980).
49. J. L. Gardner and J.A.R. Samson, J. Electron Spectrosc. 13:7 (1978).

50. R. R. Lucchese and B. V. McKoy, J. Phys. B 14:L629 (1981).
51. T. A. Carlson, M. O. Krause, D. Mehaffy, J. W. Taylor, F. A. Grimm, and J. D. Allen, J. Chem. Phys. 73:6056 (1980).
52. D. Dill, J. Welch, J. L. Dehmer, and J. Siegel, Phys. Rev. Lett. 43:1236 (1979).
53. J. L. Dehmer, J. Siegel, and D. Dill, J. Chem. Phys. 69:5205 (1978).
54. R. E. Kennerly, R. A. Bonham, and J. McMillan, J. Chem. Phys. 70:2039 (1979).
55. R. E. Kennerly, Phys. Rev. A 21:1876 (1980).
56. J. L. Dehmer, J. Siegel, J. Welch, and D. Dill, Phys. Rev. A 21:101 (1979).
57. Z. Pavlovic, M.J.W. Boness, A. Herzenberg, and G. J. Shulz, Phys. Rev. A 6:676 (1972).
58. D. G. Truhlar, S. Trajmar, and W. Williams, J. Chem. Phys. 57:3250 (1972).
59. A. Chutjian, D. G. Truhlar, W. Williams, and S. Trajmar, Phys. Rev. Lett. 29:1580 (1972).
60. J. R. Rumble, D. G. Truhlar, and M. A. Morrison, J. Phys. B 14:L301 (1981).
61. A bibliography of inner-shell spectra is given by A. P. Hitchcock, J. Electron Spectrosc. 25:245 (1982).
62. J. A. Stephens and D. Dill, Phys. Rev. A 31:1968 (1985).
63. G. V. Marr, J. M. Morton, R. M. Holmes, and D. G. McCoy, J. Phys. B 12:43 (1979).
64. M. Y. Adam, P. Morin, P. Lablanquie, and I. Nenner, paper presented at International Workshop on Atomic and Molecular Photoionization, Fritz-Haber-Institut der Max-Planck-Gesellschaft, Berlin, W. Germany, 1983 (unpublished).
65. S. H. Southworth, A. C. Parr, J. E. Hardis, and J. L. Dehmer, Phys. Rev. A 33:1020 (1986).
66. B. Basden and R. R. Lucchese, Phys. Rev. A 34:5158 (1986).
67. J. L. Dehmer, A. C. Parr, S. Wallace, and D. Dill, Phys. Rev. A 26:3283 (1982).
68. A. Gerwer, C. Asaro, B. V. McKoy, and P. W. Langhoff, J. Chem. Phys. 72:713 (1980).
69. G. Raseev, H. Lefebvre-Brion, H. Le Rouzo, and A. L. Roche, J. Chem. Phys. 74:6686 (1981).
70. P. M. Dittman, D. Dill, and J. L. Dehmer, J. Chem. Phys. 76:5703 (1982).
71. P. Morin, I. Nenner, M. Y. Adam, M. J. Hubin-Franskin, J. Delwiche, H. Lefebvre-Brion, and A. Giusti-Suzor, Chem. Phys. Lett. 92:609 (1982).
72. F. Grimm, T. A. Carlson, W. B. Dress, P. Agron, J. O. Thomson, and J. W. Davenport, J. Chem. Phys. 72:3041 (1980).
73. T. Gustafsson, E. W. Plummer, D. E. Eastman, and W. Gudat, Phys. Rev. A 17:175 (1978).
74. T. A. Carlson, M. O. Krause, F. A. Grimm, J. D. Allen, D. Mehaffy, P. R. Keller, and J. W. Taylor, Phys. Rev. A 23:3316 (1981).
75. P. W. Langhoff, T. N. Rescigno, N. Padial, G. Csanak, and B. V. McKoy, J. Chem. Phys. 77:589 (1980).
76. F. A. Grimm, J. D. Allen, T. A. Carlson, M. O. Krause, D. Mehaffy, P. R. Keller, and J. W. Taylor, J. Chem. Phys. 75:92 (1981).
77. R. R. Lucchese and B. V. McKoy, J. Phys. Chem. 85:2166 (1981).
78. N. Padial, G. Csanak, B. V. McKoy, and P. W. Langhoff, Phys. Rev. A 23:218 (1981).
79. R. R. Lucchese and B. V. McKoy, Phys. Rev. A 26:1406 (1982).
80. P. Roy, I. Nenner, M. Y. Adam, J. Delwiche, M. J. Hubin Franksin, P. Lablanquie, and D. Roy, Chem. Phys. Lett. 109:607 (1984).
81. T. Gustafsson, Phys. Rev. A 18:1481 (1978).

82. H. J. Levinson, T. Gustafsson, and P. Soven, Phys. Rev. A 19:1089 (1979).
83. J. L. Dehmer, A. C. Parr, S. H. Southworth, and D. M. P. Holland, Phys. Rev. A 30:1783 (1984).
84. T. A. Ferrett, D. W. Lindle, P. A. Heimann, H. G. Kerkhoff, U. E. Becker, and D. A. Shirley, Phys. Rev. A 34:1916 (1986), and to be published.
85. T. A. Ferrett, Ph.D. Thesis, U. California, Berkeley (1986).
86. L. S. Cederbaum, W. Domcke, J. Schirmer, and W. von Niessen, Phys. Scr. 21:481 (1980).
87. S. Krummacher, V. Schmidt, and F. Wulleumier, J. Phys. B 13:3993 (1980).
88. P. W. Langhoff, S. R. Langhoff, T. N. Rescigno, J. Schirmer, L. S. Cederbaum, W. Domcke, and W. von Niessen, Chem. Phys. 58:71 (1981).
89. F. Sette, J. Stöhr, and A. P. Hitchcock, Chem. Phys. Lett. 110:517 (1984); J. Chem. Phys. 81:4906 (1984).
90. M. N. Piancastelli, D. W. Lindle, T. A. Ferrett, and D. A. Shirley, J. Chem. Phys. 86:2765 (1987).
91. D. L. Lynch, S. N. Dixit, and V. McKoy, J. Chem. Phys. 84:5504 (1986).
92. M. Braunstein and V. McKoy, J. Chem. Phys. 87:224 (1987).
93. See, e.g., P. W. Langhoff in Chapter 7 of Ref. 2.
94. F. A. Gianturco, C. Guidotti, and U. Lamanna, J. Chem. Phys. 57:840 (1972).
95. D. Dill, J. R. Swanson, S. Wallace, and J. L. Dehmer, Phys. Rev. Lett. 45:1393 (1980).
96. U. Becker, R. Hölzel, H. G. Kerkhoff, B. Langer, D. Szostak, and R. Wehlitz, Phys. Rev. Lett. 56:1455 (1986).